47th AIAA Aerospace Sciences Meeting Including The New Horizons Forum and Aerospace Exposition
5 - 8 January 2009, Orlando, Florida

AIAA 2009-1316

Nonequilibrium Aerothermodynamics of Sharp Leading Edges

Andrew J. Lofthouse*
U.S. Air Force Institute of Technology, Wright-Patterson AFB, OH, 45433

Iain D. Boyd†
The University of Michigan, Ann Arbor, MI, 48109

This paper presents a detailed computational study quantifying the effects of nonequilibrium on the surface properties of a hypersonic vehicle by comparing Navier-Stokes-based Computational Fluid Dynamics (CFD) and direct simulation Monte Carlo (DSMC) simulation results for the flow about a wedge. Physical submodels contained in both computational methods are ensured to be as equivalent as possible. Translational nonequilibrium effects are isolated by considering a monatomic gas, argon. Thermal nonequilibrium effects are included by considering a diatomic gas, nitrogen. Several different flow regimes are considered, from the continuum into the transitional (freestream Knudsen numbers are 0.002, 0.01, 0.05 and 0.25), with Mach numbers of 10 and 25. Effects on surface properties (total drag and peak heat transfer rate) are quantified at each flow condition. Flow field properties are also compared. Continuum breakdown parameter values are compared with other flow and surface properties. Previous work studied flows of argon and nitrogen about a cylinder. This paper extends the work for flows about a wedge, having an infinitely sharp leading edge. Total drag differences range between 2% and 34%, mostly due to friction force differences. Peak heating differences are between 70% and 100%; DSMC predicts a much higher temperature near the leading edge than CFD.

I. Introduction

The design of hypersonic vehicles requires accurate prediction of the surface properties. These quantities are typically the heat flux, pressure and shear stress. During it's trajectory through an atmosphere, a hypersonic vehicle will experience vastly different flow regimes due to the variation of atmospheric density with altitude. In addition, the high temperatures encountered due to the high velocities cause dissociation and ionization of the atmospheric gases. Reproduction of these varied flow conditions in ground-based laboratory facilities is both expensive and technically challenging. Thus, there is an extremely important role for computational models in the development of hypersonic vehicles.

In the continuum regime flows around hypersonic vehicles can be accurately simulated using traditional Computational Fluid Dynamics (CFD) by solving either the Euler or preferably the Navier-Stokes (NS) equations. In the rarefied flow regime the flow can be computed using the direct simulation Monte Carlo (DSMC) method.[2] The DSMC method does not depend assumptions involving a small perturbation from equilibrium and hence is more accurate than CFD methods for non-equilibrium flows. Generally speaking, CFD methods for solving the NS equations are about an order of magnitude faster than the DSMC method. Note that in continuum regimes, locally a flow may behave like a rarefied flow if the local characteristic length scale is very small.

*Assistant Professor, Department of Aeronautics and Astronautics, 2950 Hobson Way; Andrew.Lofthouse@afit.edu. Senior Member AIAA.

†Professor, Department of Aerospace Engineering, 1320 Beal Avenue; iainboyd@umich.edu. Associate Fellow AIAA.

"The views expressed in this paper are those of the author and do not reflect the official policy or position of the United States Air Force, Department of Defense, or the U.S. Government"

The areas of the flow where the continuum hypothesis breaks down (or equivalently, where the flow is no longer in local thermodynamic equilibrium), can be quantified by the use of a continuum breakdown parameter. While there have been several breakdown parameters presented in the literature,[1,6,8,19] the one that appears to be most appropriate for hypersonic compressible flows is the gradient-length local (GLL) Knudsen number[5,22]

$$\mathrm{Kn}_{\mathrm{GLL}} = \frac{\lambda}{Q}\left|\frac{dQ}{dl}\right| \tag{1}$$

where the derivative is taken in the direction of the maximum gradient, and Q is some quantity of interest such as density, pressure, temperature or velocity magnitude. When calculating $\mathrm{Kn}_{\mathrm{GLL}}$ based on velocity magnitude, the gradient is normalized by the maximum of the local velocity magnitude and the local speed of sound. It is generally assumed that continuum breakdown occurs whenever $\mathrm{Kn}_{\mathrm{GLL}}$ (based on the CFD solution) is greater than 0.05.

Previous work[11–13] sought to quantify the errors in CFD predictions of surface properties of a hypersonic blunt body by comparing those solutions with DSMC solutions for a variety of flows in the transitional regime. The maximum $\mathrm{Kn}_{\mathrm{GLL}}$ was also computed in each case to determine the effect of continuum breakdown on the surface properties. The cases considered were Mach 10 and Mach 25 flows of argon and nitrogen around a cylinder, with various slip boundary conditions imposed at the wall.

This paper now considers the flow about a wedge with a sharp leading-edge. The cylinder simulations exhibited a typical blunt-body hypersonic flow with an unattached shock, followed by a high-temperature, low velocity shock layer. Regions of high nonequilibrium were found in the shock, the boundary layer and the wake. A sharp leading-edge body, on the other hand, is characterized by an attached shock, and supersonic velocities throughout the flow (with the exception of the boundary layer). Regions of high nonequilibrium are expected near the leading-edge and in the boundary layer and wake.

II. Background and Simulation Procedure

This investigation considers a hypersonic flow of nitrogen over a 10-deg half-angle wedge. The height of the base is 12-inches, equivalent to the diameter of the cylinder previously considered. Two different free stream velocities are used that correspond to Mach 10 and Mach 25 flows (U_∞ = 2883 m/s and 7208 m/s, respectively). The wall temperature is held constant at 500 K (Mach 10) and 1500 K (Mach 25). The free stream density of the flow is varied such that several different regimes are considered, from the continuum through the transitional to the rarefied regime, as shown in Table 1. Knudsen numbers are calculated based on freestream conditions and the wedge base height, using the hard-sphere model for the mean free path calculation. Surface and flow field properties for this flow are presented from two different computational approaches.

Table 1. Flow regimes considered.

Kn_∞ *	n $[\mathrm{particles/m^3}]$	ρ_∞ (Ar) $[\mathrm{kg/m^3}]$	ρ_∞ (N_2) $[\mathrm{kg/m^3}]$	Re **
0.002	2.124×10^{21}	1.408×10^{-4}	9.872×10^{-5}	20,000
0.01	4.247×10^{20}	2.818×10^{-5}	1.974×10^{-5}	4,000
0.05	8.494×10^{19}	5.636×10^{-6}	3.949×10^{-6}	800
0.25	1.699×10^{19}	1.127×10^{-6}	7.897×10^{-7}	160

* Based on hard-sphere mean free path.

** Based on cylinder diameter and Mach 25.

DSMC results are provided from the MONACO code[7] for the flow conditions mentioned above. MONACO is a general 2D/3D, object-oriented, cell-based, parallel implementation of the DSMC method. It uses the Variable Hard Sphere (VHS) and Variable Soft Sphere collision models.[2,10] It also includes variable vibrational[20] and rotational[4] energy exchange probability models.

All MONACO solutions are generated using a fixed wall temperature at 500 K and 1500 K. Bird's variable hard sphere model is used.[2] The VHS parameters used in the DSMC computations are those for standard argon and nitrogen, as shown in Table 3. The details of the vibrational relaxation model as implemented in

Table 2. Boundary conditions.

Mach	U_∞ (Ar) [m/s]	U_∞ (N_2) [m/s]	T_∞ [K]	T_{wall} [K]
10	2624	2883	200	500
25	6585	7208	200	1500

MOANCO was previously discussed.[12]

Table 3. Variable hard sphere (VHS) model parameters for argon and nitrogen used in the computational simulations.

Species	ω	T_{ref} [K]	d_{ref} [m]
Ar	0.734	1000	3.595×10^{-10}
N_2	0.7	290	4.110×10^{-10}

The mesh used for the final solution is adapted such that the cell sizes are on the order of one mean free path or smaller, with the exceptions of the Kn = 0.002 and Kn = 0.01 cases (where the subcell method is used to select particles for collisions to ensure physical accuracy[2]). The flow near the leading-edge exhibits an extremely high amount of nonequilibrium. Thus, the mesh around the leading-edge in each case is adapted such that the cell size is about 10-40% of a mean free path in order to sufficiently resolve the flow details.

CFD results are obtained through solution of the Navier-Stokes equations. The CFD results are obtained using the Michigan Aerothermodynamic Navier-Stokes (LeMANS) code, developed at the University of Michigan for the simulation of hypersonic reacting flow-fields.[16,17] LeMANS is a general two-dimensional, three-dimensional and axisymmetric, parallel, unstructured, finite-volume CFD code capable of simulating gases in thermal and chemical non-equilibrium. A two-temperature model is used to account for the non-equilibrium between the vibrational and the translational-rotational modes,[15] with the energy exchange rates modeled using the Landau-Teller model.[21] Although transport properties can be computed using Wilke's[23] and Blottner's[3] models, it is important to ensure identical transport properties are used with both models, hence the VHS model viscosity is used directly in the CFD calculations.[18] The thermal conductivity is determined using Eucken's relation.[16]

All LeMANS solutions are generated assuming an isothermal wall at 500 K (Mach 10) and 1500 K (Mach 25). Slip boundary conditions based on those presented by Gökçen[9] are implemented. Vibrational relaxation rates based on the Millikan and White[14] correlations to the Landau-Teller model, along with the Park correction,[15] are used in the simulations, as detailed previously.[12]

A mesh-independence study is conducted in each case to determine the final mesh resolution used. For the cylinder it was determined that the wall-normal spacing had the most effect on mesh-independence of the surface properties. For the wedge, mesh refined near the leading edge in the wall-parallel direction also has a large effect on the surface properties, due to the large gradients in that area. For the wedge, in addition to the wall-normal mesh refinement, the number of nodes near the leading edge is successively doubled. A mesh-independent solution is defined as one for which the total drag and peak heat transfer rate change by 1% or less when using the more refined mesh.

In the results that follow, the surface properties are presented in terms of non-dimensional coefficients, as defined in Eqs. 2 - 4. The surface properties in each case are plotted as a function of the distance, S, along the wedge surface, normalized by the length, L, of the top surface. Thus, $S/L = 1$ is the location of the wedge shoulder and the beginning of the wake of the flow.

$$C_P = \frac{p - p_\infty}{\frac{1}{2}\rho_\infty U_\infty^2} \tag{2}$$

$$C_F = \frac{\tau}{\frac{1}{2}\rho_\infty U_\infty^2} \tag{3}$$

$$C_H = \frac{q}{\frac{1}{2}\rho_\infty U_\infty^3} \tag{4}$$

Along with the surface properties, the maximum value of Kn_{GLL} at the surface (based on the CFD solution) is plotted in each case.

III. Argon

The flow of argon about the wedge is considered first. Table 4 summarizes the total drag predicted by CFD and DSMC. There is reasonable agreement at the lowest Knudsen number, with less than 2% difference for both Mach 10 and Mach 25. However, as the flow becomes more rarefied, the differences increase, with the maximum differences of 20% for Mach 10 and over 34% for Mach 25 seen for the Kn = 0.25 cases.

Table 4. Total drag for flow of argon about a wedge.

Kn_∞	Mach 10			Mach 25		
	Drag/Length [N/m] (% Difference)					
	DSMC	CFD		DSMC	CFD	
0.002	38.89	39.42	(1.4%)	252.3	257.2	(1.9%)
0.01	13.66	14.22	(4.1%)	92.74	99.86	(7.7%)
0.05	5.091	5.639	(10.8%)	34.39	40.13	(16.7%)
0.25	1.709	2.051	(20.0%)	10.35	13.91	(34.4%)

Figure 1 illustrates the percentage of total drag due to pressure and friction forces, for both DSMC and CFD. It is significant to note that as the Knudsen number increases, the percentage of total drag due to friction increases from about 50% at Kn = 0.002 to over 80% at Kn = 0.25 for Mach 10. For Mach 25, an even larger portion of the total drag is due to friction forces—nearly 60% at Kn = 0.002 to almost 90% at Kn = 0.25. This is contrasted with the cylinder in the previous work where friction forces accounted for, at most, 20% of the total drag (at Kn = 0.25); the vast majority of the drag was due to pressure forces. It is also significant to note, as shown in Figure 2, that the difference in predicted total drag between CFD and DSMC is due mostly to the differences predicted in the friction forces, as was also the case with the cylinder.

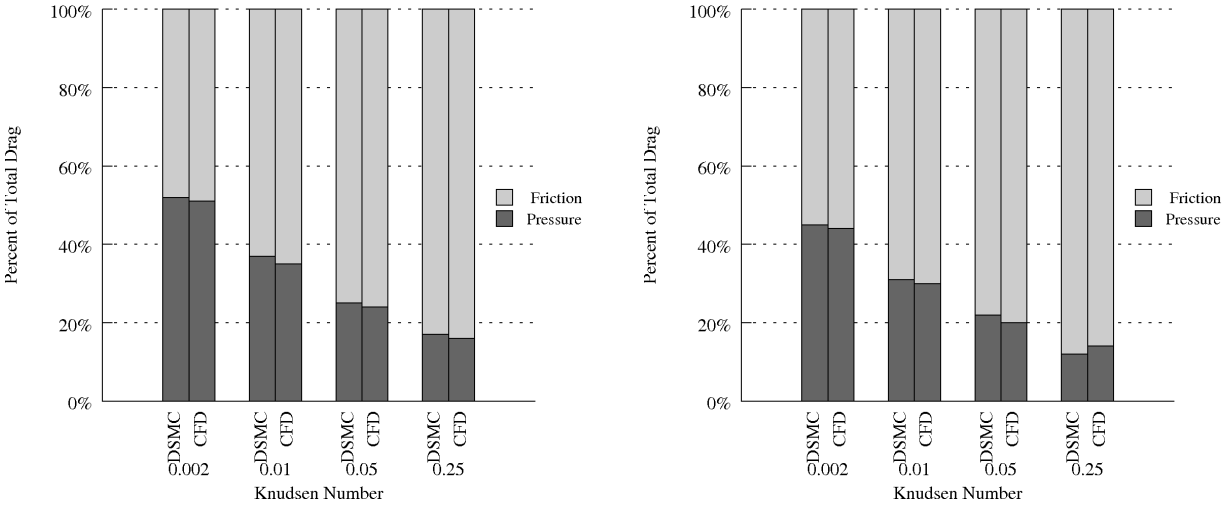

(a) Mach 10 (b) Mach 25

Figure 1. Percentage of total drag due to pressure and friction for flow of argon about a wedge. In contrast to the cylinder cases, here friction forces account for most of the drag.

In all cases, CFD overpredicts the total drag. Although these CFD simulations make use of the Gökçen slip conditions (which gave very reasonable results for total drag in the case of the cylinder), the differences

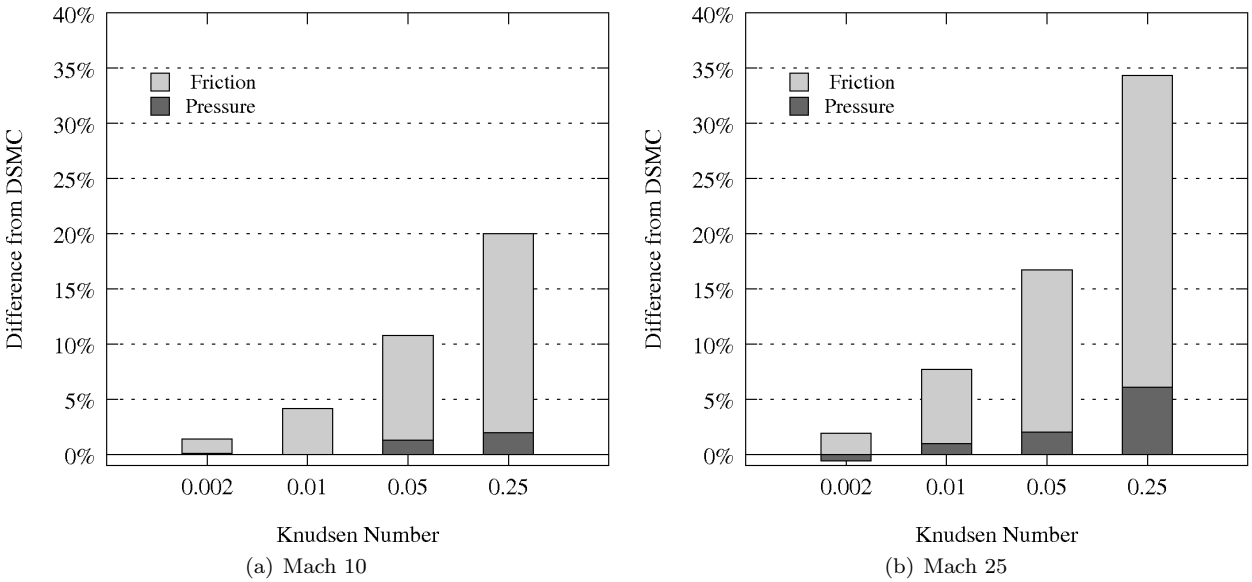

(a) Mach 10

(b) Mach 25

Figure 2. Total drag difference from DSMC predicted by CFD for flow of argon about a wedge.

in total drag predictions here are similar in magnitude to the disagreement produced when using the no-slip boundary conditions in the case of the cylinder. This increased disagreement for the wedge is simply due to the fact that a larger percentage of the total drag is due to friction forces, and the shear stress is more sensitive to continuum breakdown due to rarefaction than is pressure; hence there is more disagreement in the total drag predictions for the wedge than there was for the cylinder.

The peak heat transfer rate predicted by CFD and DSMC is summarized in Table 5, and the differences are shown graphically in Figure 3. Here the differences between CFD and DSMC for all but the most rarefied cases are near 70%. It will be shown below that for the Kn = 0.25 cases the peak heating is predicted by CFD to occur at the shoulder of the wedge rather than at the leading edge for these cases—the differences in peak heating at the leading edge is 100%. In all cases, CFD also underpredicts the maximum heat flux. These differences are significantly larger than were seen with the cylinder, and this is the most striking difference between surface predictions of a blunt body compared with those of a sharp-leading edge body. It will also be shown below that DSMC predicts a very high temperature region at the leading edge in all cases; CFD is unable to match these flow conditions due to the large effects of nonequilibrium present near the leading edge.

Table 5. Peak heat transfer rate for flow of argon about a wedge. The large differences between CFD and DSMC are due to the failure of CFD to predict the high temperatures at the leading edge.

Kn_∞	**Mach 10**			**Mach 25**		
	Peak Heating $\left[kW/m^2\right]$ (% Difference)					
	DSMC	CFD		DSMC	CFD	
0.002	239.5	76.03	(-68.3%)	3807.	1143.	(-70.0%)
0.01	47.48	15.38	(-67.6%)	754.2	231.1	(-69.4%)
0.05	9.451	3.109	(-67.1%)	151.0	46.50	(-69.2%)
0.25	1.902	1.247	(-100.0%)	31.76	26.04	(-100.0%)

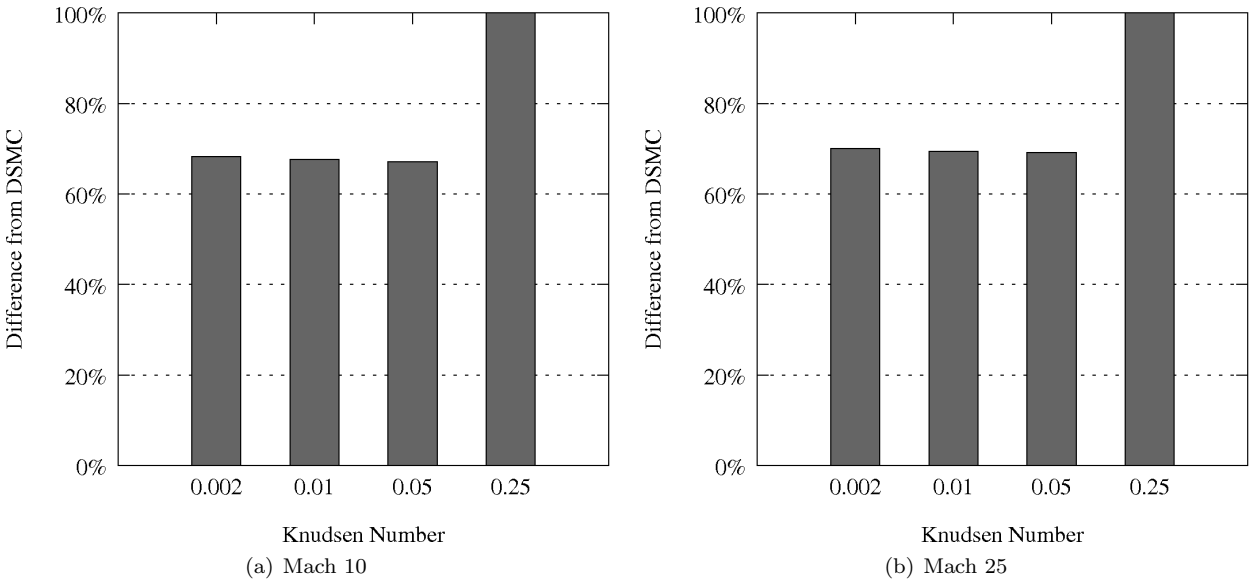

(a) Mach 10 (b) Mach 25

Figure 3. Peak heat transfer rate difference from DSMC predicted by CFD for flow of argon about a wedge. The large differences in peak heating are due to the failure of CFD to predict the high temperatures at the leading edge.

A. Continuum Breakdown

As before, the breakdown parameter is calculated using both the CFD and the DSMC solutions according to Equation 1. For the case of a wedge in a hypersonic flow of a simple gas, breakdown of the continuum hypothesis is expected in regions of high gradients (such as the shock and boundary layer, and especially near the leading edge) and in regions of rarefaction (such as the wake). The amount of continuum breakdown is again expected to increase as the gas flow becomes more rarefied.

The maximum $\mathrm{Kn}_{\mathrm{GLL}}$ for the Mach 10 cases is plotted in Figures 4 (Mach 25 is similar). The detail of the flow near the leading-edge is shown in the inset. In these figures, the maximum gradient length local Knudsen number is computed from the DSMC (top) and CFD (bottom) solutions. The light gray regions correspond to $\mathrm{Kn}_{\mathrm{GLL}} < 0.05$, dark gray regions correspond to $\mathrm{Kn}_{\mathrm{GLL}} < 1.0$, and black regions correspond to $\mathrm{Kn}_{\mathrm{GLL}} > 1.0$.

For the Kn = 0.002 cases, there is a significant amount of nonequilibrium (as quantified by a breakdown parameter value exceeding 0.05, and represented by dark gray) present in the shock, the boundary layer and the wake. The size of this region of nonequilibrium grows as the flow becomes rarefied, until it encompasses nearly the entire computational domain at Kn = 0.25. This is very similar to what was seen in the flow around the cylinder. Note, however, the large amount of nonequilibrium near the leading-edge, as shown in the inset of Figure 4, and near the shoulder of the wedge as the flow expands into the wake. As the flow becomes more rarefied, these regions of severe nonequilibrium grow larger. It will be seen below that the region of high nonequilibrium near the leading-edge has a much more significant impact on the surface property predictions, even for the cases that are within the continuum regime, than does the wake region.

B. Flow Field Properties

The temperature fields predicted by both CFD and DSMC for the Mach 10 flow can be seen in Figure 5. The temperature field predicted by both methods seems to agree in the majority of the computational domain for Kn = 0.002, Kn = 0.01 and even Kn = 0.05, with some differences in the wake. However, near the leading edge (see insets), DSMC predicts a much higher temperature than CFD (the peak temperatures are about 3,000-3,400 K for Mach 10 and 16,000-20,000 K for Mach 25). For Kn = 0.002, the DSMC temperature at the leading edge is about 40% higher than the CFD temperature, and the peak DSMC temperature is about 15% higher than the peak CFD temperature. As the Knudsen number increases, the difference in temperature at the leading edge increases to nearly 50% for Kn = 0.25. Although DSMC always predicts the peak temperature to be at the leading edge, CFD predicts a higher temperature in the wake for these most

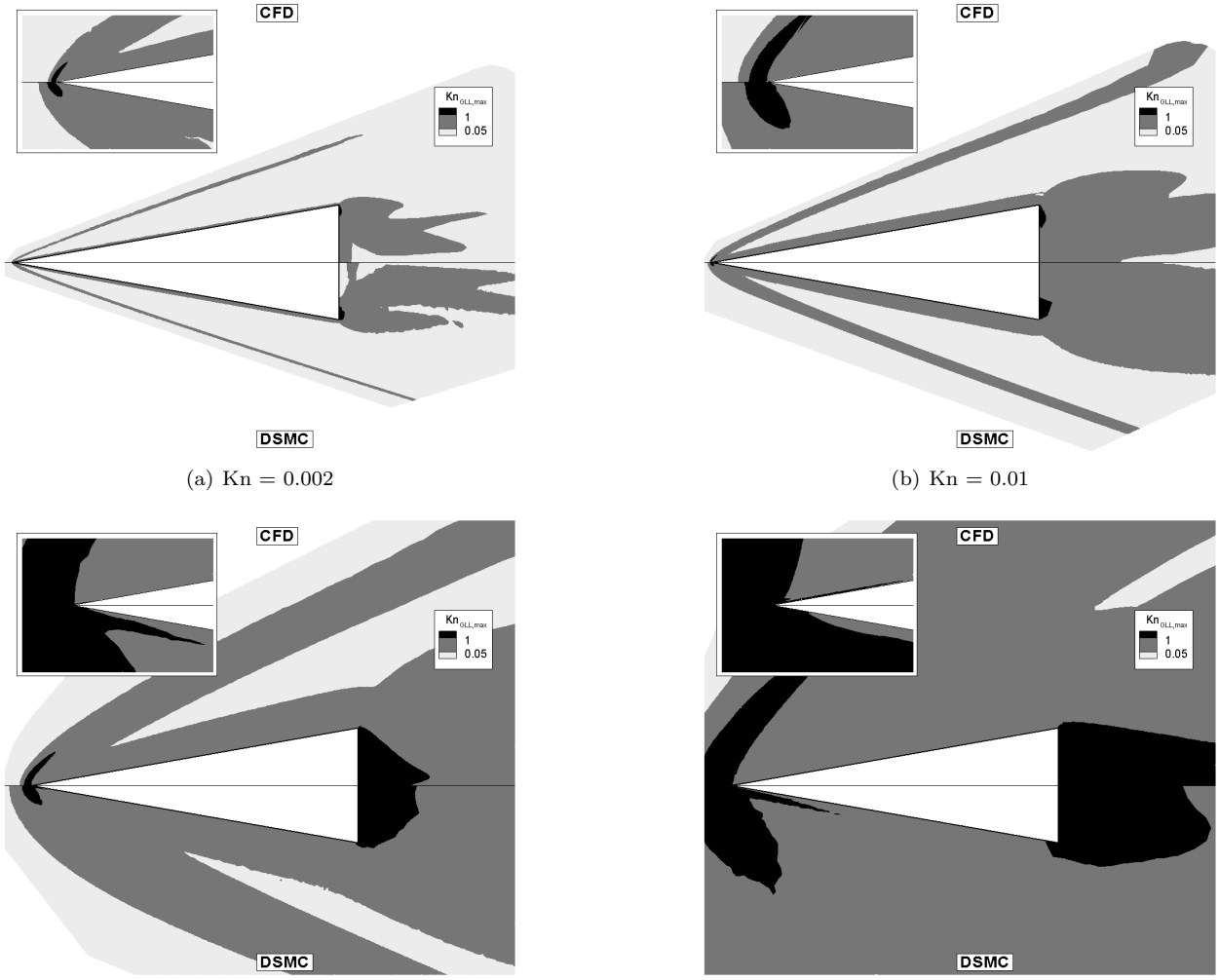

(a) Kn = 0.002

(b) Kn = 0.01

(c) Kn = 0.05

(d) Kn = 0.25

Figure 4. $\mathrm{Kn_{GLL}}$ **field for a Mach 10 flow of argon about a wedge. The light gray regions correspond to** $\mathrm{Kn_{GLL}} < 0.05$**, dark gray regions correspond to** $\mathrm{Kn_{GLL}} < 1.0$**, and black regions correspond to** $\mathrm{Kn_{GLL}} > 1.0$**. Note that the minimum value of** $\mathrm{Kn_{GLL}}$ **for the black regions is an order of magnitude greater than those for the cylinder**

rarefied cases. It is clear that CFD cannot accurately predict the temperature gradients near the leading edge even for the highest density cases, causing a large difference in the predicted heat transfer rates.

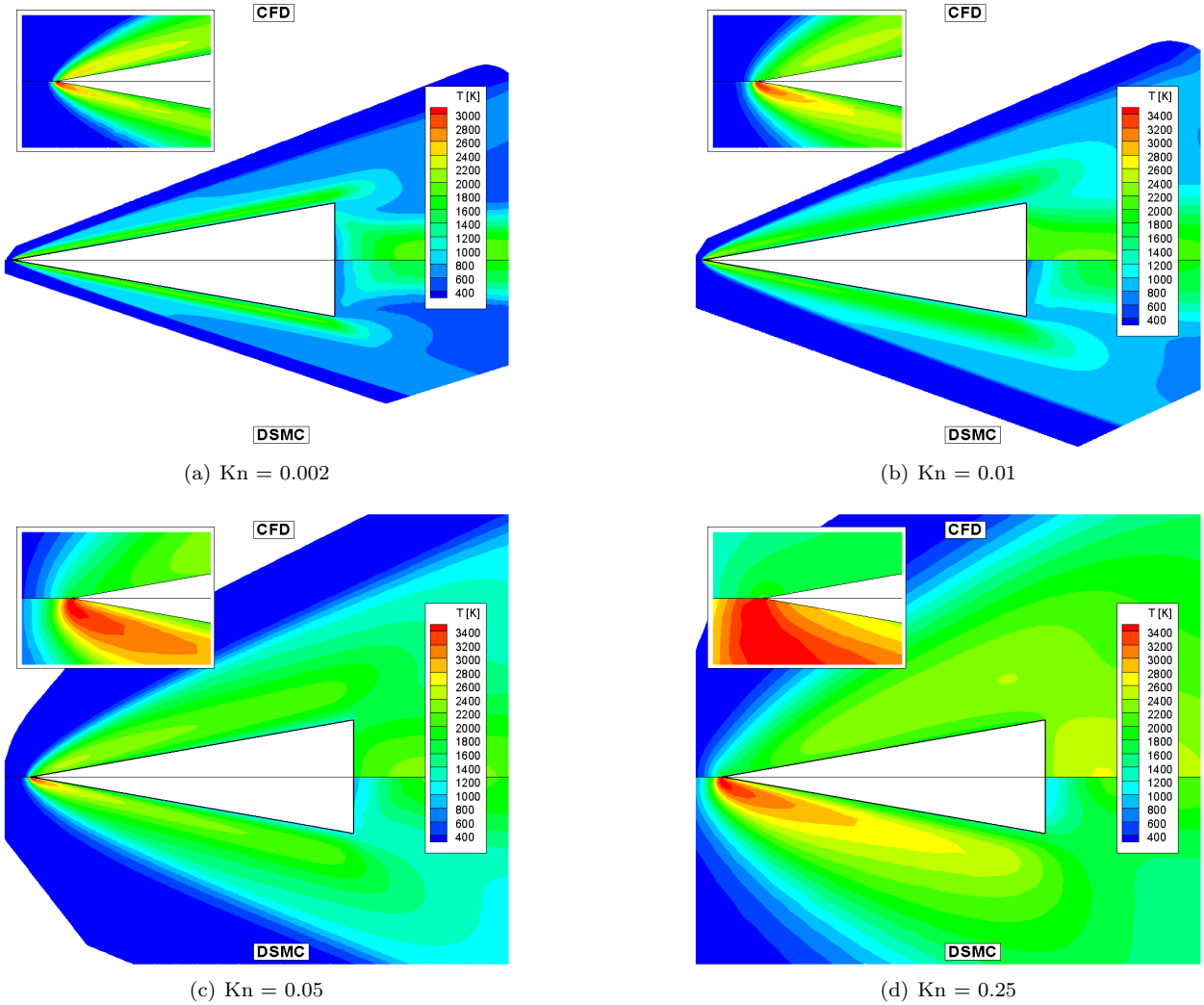

(a) Kn = 0.002

(b) Kn = 0.01

(c) Kn = 0.05

(d) Kn = 0.25

Figure 5. Temperature field for a Mach 10 flow of argon about a wedge. DSMC predicts a much higher temperature than CFD near the leading edge (inset). Note that CFD predicts a higher temperature in the wake than near the leading edge for Kn = 0.25, while DSMC predicts a maximum temperature at the leading edge.

C. Surface Properties

The surface property distributions (pressure, shear stress and heat flux) for each case are now examined. The surface pressure, in the form of a pressure coefficient, is shown for Mach 10 in Figure 6. For the blunt-body, the surface pressure was the least sensitive to nonequilibrium of all the surface properties; for the wedge, however, there are significant differences in the pressure distributions, even at Kn = 0.002. Although there are significant levels of nonequilibrium in the wake as well as at the leading edge, as shown by Figure 4, the pressure is affected primarily at the leading edge. The overall CFD pressure distribution agrees qualitatively with DSMC for all but the Kn = 0.25 case, but the peak pressure at the leading edge is overpredicted by CFD. The distributions also start to differ in the wake for Kn = 0.05 and Kn = 0.25, with CFD predicting a large spike in the pressure at $S/L = 1$ as the flow begins to expand into the wake. In all cases, CFD tends to overpredict the pressure, hence there is some effect of the pressure on the overall overprediction of total drag by CFD, although this effect is not as great as that of shear stress, as was shown in Figure 2.

The shear stress on the wedge surface for the Mach 10 cases is seen in Figure 7. Here, there is a large

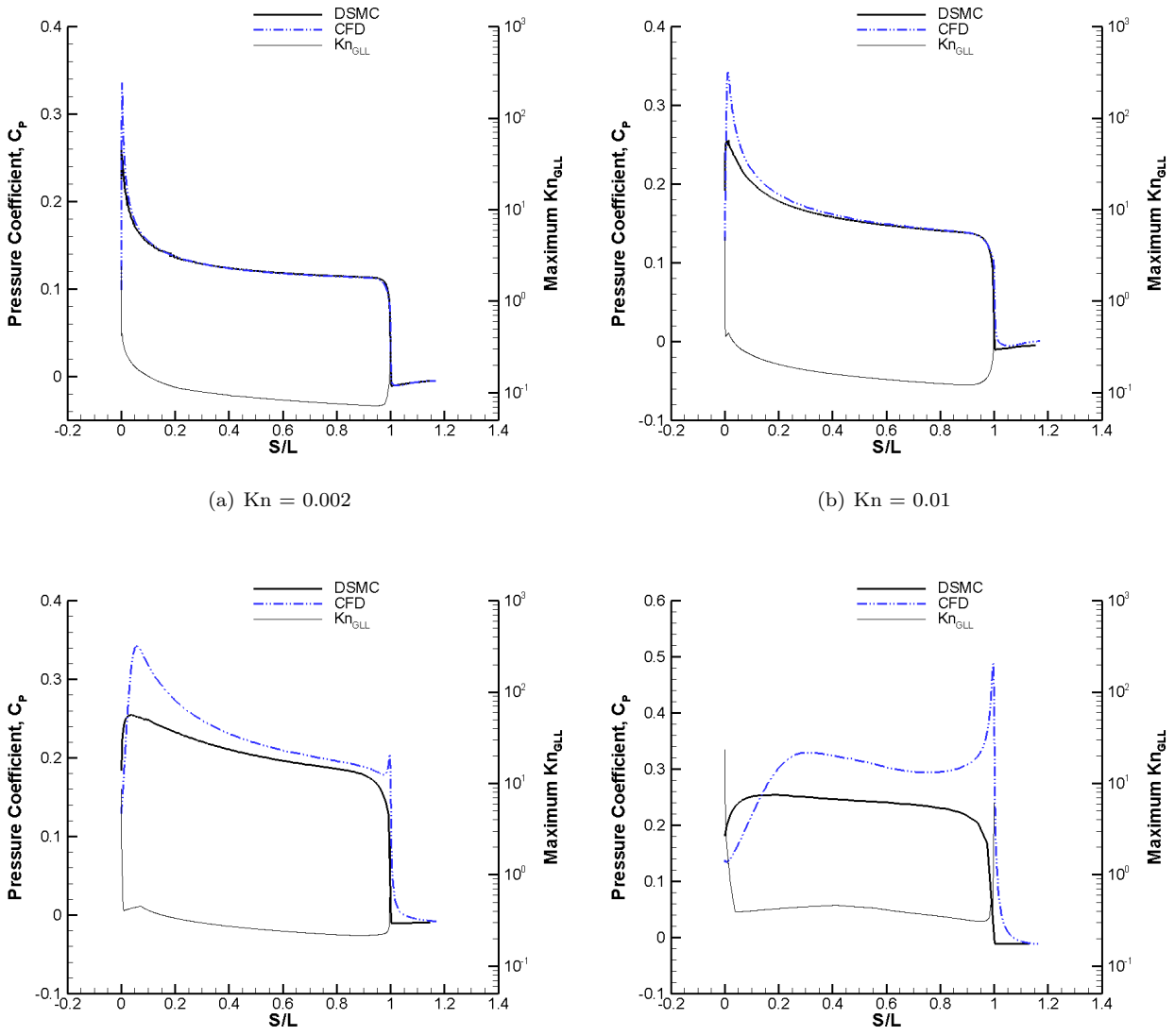

(a) Kn = 0.002

(b) Kn = 0.01

(c) Kn = 0.05

(d) Kn = 0.25

Figure 6. Surface pressure coefficient for Mach 10 flow of argon about a wedge. The maximum value of $\mathrm{Kn}_{\mathrm{GLL}}$ near the surface plotted on the right axis. The distance along the surface (including the base), S, is normalized by the top surface length, L.

spike in the CFD shear stress right at the leading edge that is not shown in the figures. The maximum friction coefficient at that point is annotated in each case. This peak ranges from a fairly low value of 0.43 for Mach 25, Kn = 0.002 (which is not much different from the peak DSMC value) to a maximum of 41.3 for Mach 25, Kn = 0.25 (compared to about 0.36 for DSMC). Other than this peak at the leading edge, there are fewer differences in the shear stress than there were for the pressure. However, the total drag is affected most by the friction forces. This apparent paradox is explained by noting again the much larger effect that shear stress has on the total drag as seen in Figure 2.

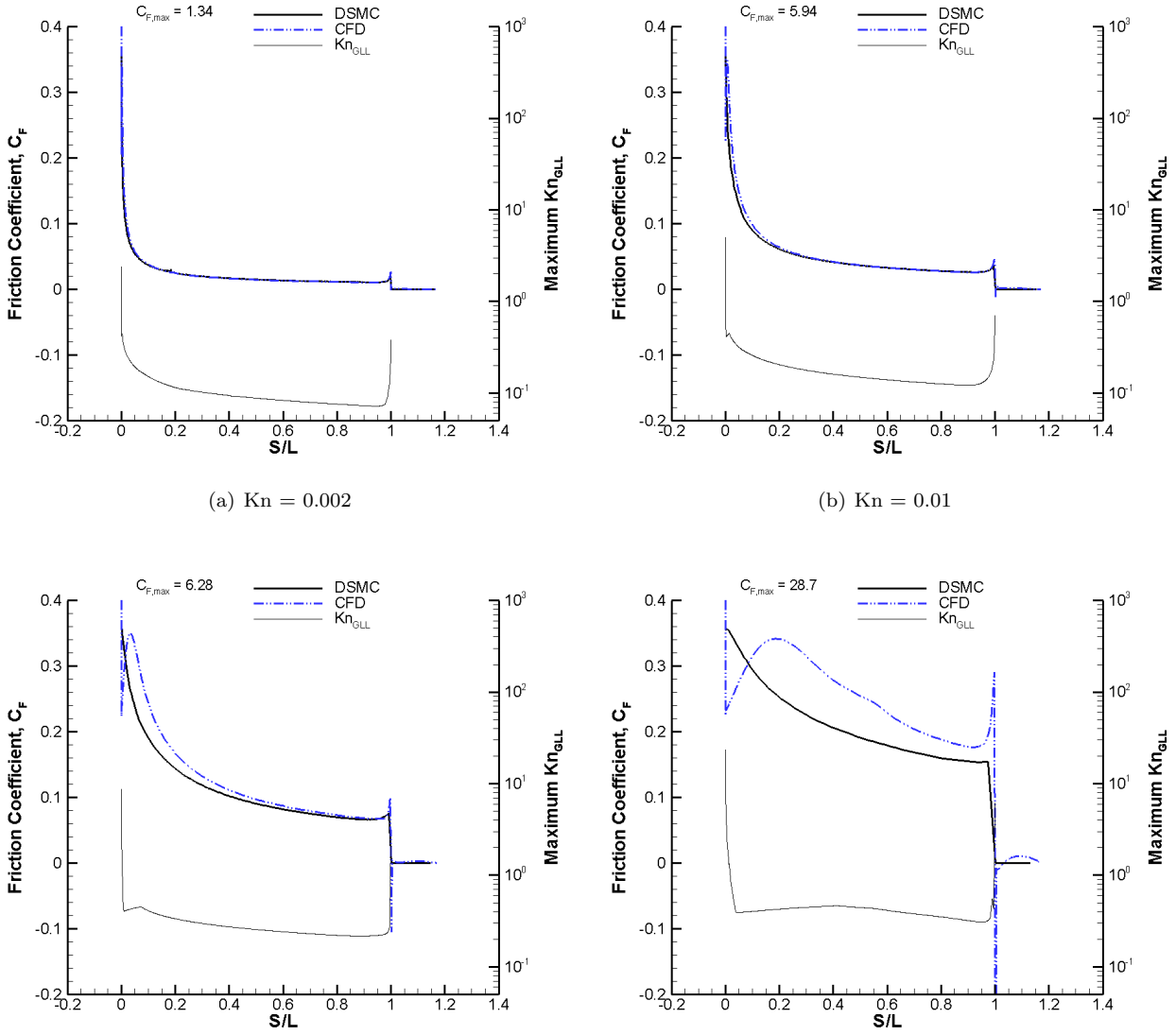

(a) Kn = 0.002

(b) Kn = 0.01

(c) Kn = 0.05

(d) Kn = 0.25

Figure 7. Surface friction coefficient for Mach 10 flow of argon about a wedge. The maximum value of $\mathrm{Kn}_{\mathrm{GLL}}$ near the surface plotted on the right axis. The distance along the surface (including the base), S, is normalized by the top surface length, L.

The peak at the leading edge does not have any significant effect on the total drag due to the small surface area on which the friction force acts. Figure 8 compares the accumulated total drag along the wedge surface due to both friction and pressure forces for the Mach 10 cases. The accumulated total drag along the surface is calculated by summing the drag from the leading edge up to each point along the surface, thus the total drag is shown at about $S/L = 1.2$. The locations where there are large differences between the CFD and DSMC drag predictions are seen where the distance between the two lines on the plots increases. Thus,

the differences in friction drag for Kn = 0.002 and Kn = 0.01 occur along the first 20% of the wedge surface. For Kn = 0.05, the area where the difference accumulates most is in the first 40-50% of the wedge surface; and for Kn = 0.25, the differences accumulate mostly between 20% and 80% of the wedge length. Note that the peak in friction coefficient at the leading edge has no significant impact on the total drag. Figure 8 (and similar plots for the Mach 25 cases) also demonstrates that:

- The contribution of friction forces to the total drag increases as the density decreases.
- There is no contribution to total drag due to friction forces in the wake.
- Pressure forces on the base of the wedge (in the wake) decrease the total drag.
- There is little disagreement in the predictions of total drag due to pressure forces for most cases.

Fairly significant disagreement in shear stress prediction for Kn = 0.05 and Kn = 0.25 is also seen at $S/L = 1$ at the sharp angle between the top wedge surface and the base.

The heat transfer rate distributions for Mach 10 are shown in Figure 9. Previously, it was shown that DSMC predicts a temperature as much as 40% higher than CFD at the leading edge. The inability of CFD to model the flow at the leading edge has a large effect on the heat flux. Although the qualitative agreement is good at Kn = 0.002, DSMC predicts a heating coefficient of nearly 0.19, while CFD predicts a much lower heating coefficient of about 0.07. As the Knudsen number increases, the DSMC peak heating coefficient remains at about 0.19 - 0.20, while the CFD peak heating coefficient remains near 0.05 - 0.06. Thus, the difference in heating rate is around 70% for most of the cases. For Kn = 0.25, CFD predicts a peak heating rate at the shoulder, with no heating predicted at the leading edge. The actual error in heating rate prediction, then, is much greater than the 35% and 18% cited in Table 5 and shown in Figure 3.

D. Slip Quantities

The velocity slip profiles along the wedge surface for the Mach 10 cases are shown in Figure 10 (Mach 25 profiles are similar). In all cases, CFD predicts a peak velocity slip of about 2000 m/s (for Mach 10) and about 5000 m/s (for Mach 25) near the leading edge, while DSMC predicts a maximum velocity slip of about 700 m/s (for Mach 10) and about 1100 m/s (for Mach 25). Past the leading edge, the velocity slip is very quickly reduced to a nearly constant finite value until the wedge shoulder, where a sharp increase is seen. For Kn = 0.002 Kn = 0.01 and even Kn = 0.05 to some extent, CFD qualitatively agrees fairly well with DSMC. However, for Kn = 0.25 this agreement worsens considerably. The locations where the disagreement is most apparent, at and near the leading edge, are also the locations where the shear stress distributions differ the most. Thus, there is a good correlation between velocity slip disagreement and shear stress disagreement.

The temperature jump profiles for Mach 10 are shown in Figure 11. The DSMC profile of temperature jump is very similar to that for velocity slip; the temperature jump is highest at the leading edge, with a gradual decrease to an almost constant value and a slight bump around the wedge shoulder. The peak temperature jump predicted by DSMC is between about 2000-2200 K (for Mach 10) and 10000-11000 K (for Mach 25). CFD agrees fairly well for Kn = 0.002, but shows large disagreements for all other cases, particularly in the wake. The CFD peak temperature jump is not much different from that of DSMC, especially for the Mach 25 cases. There does not seem to be any strong correlation between the temperature jump agreement and the disagreement between heat transfer rates.

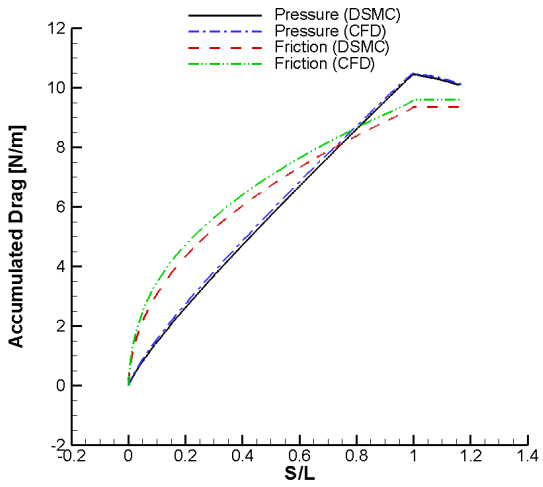

(a) Kn = 0.002

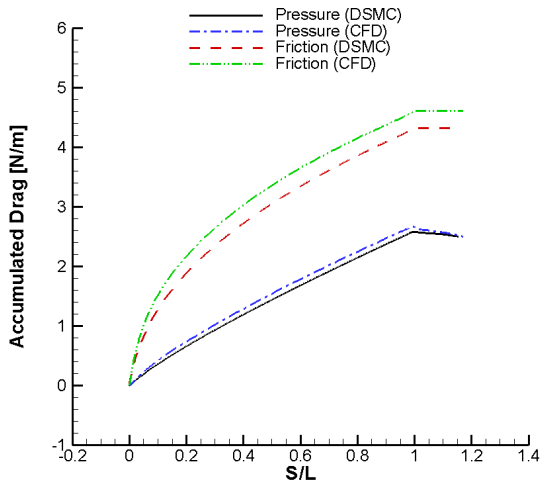

(b) Kn = 0.01

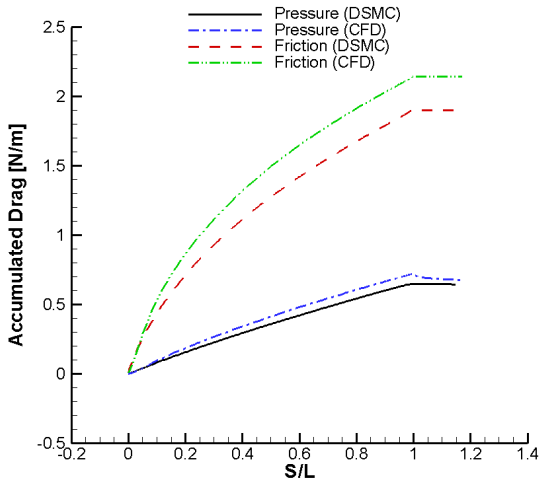

(c) Kn = 0.05

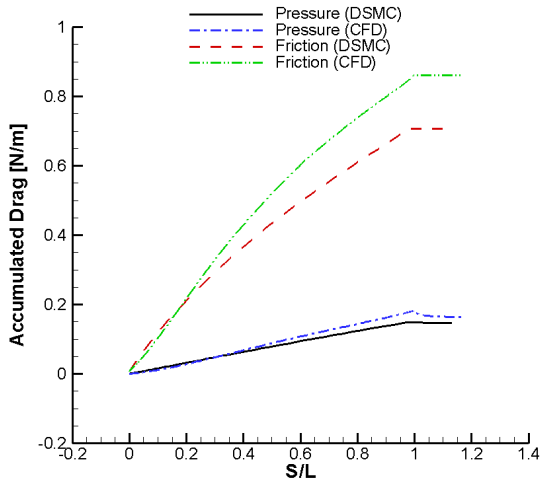

(d) Kn = 0.25

Figure 8. Contributions of pressure and skin friction forces to accumulated total drag for a Mach 10 flow of argon about a wedge. The distance along the surface (including the base), S, is normalized by the top surface length, L.

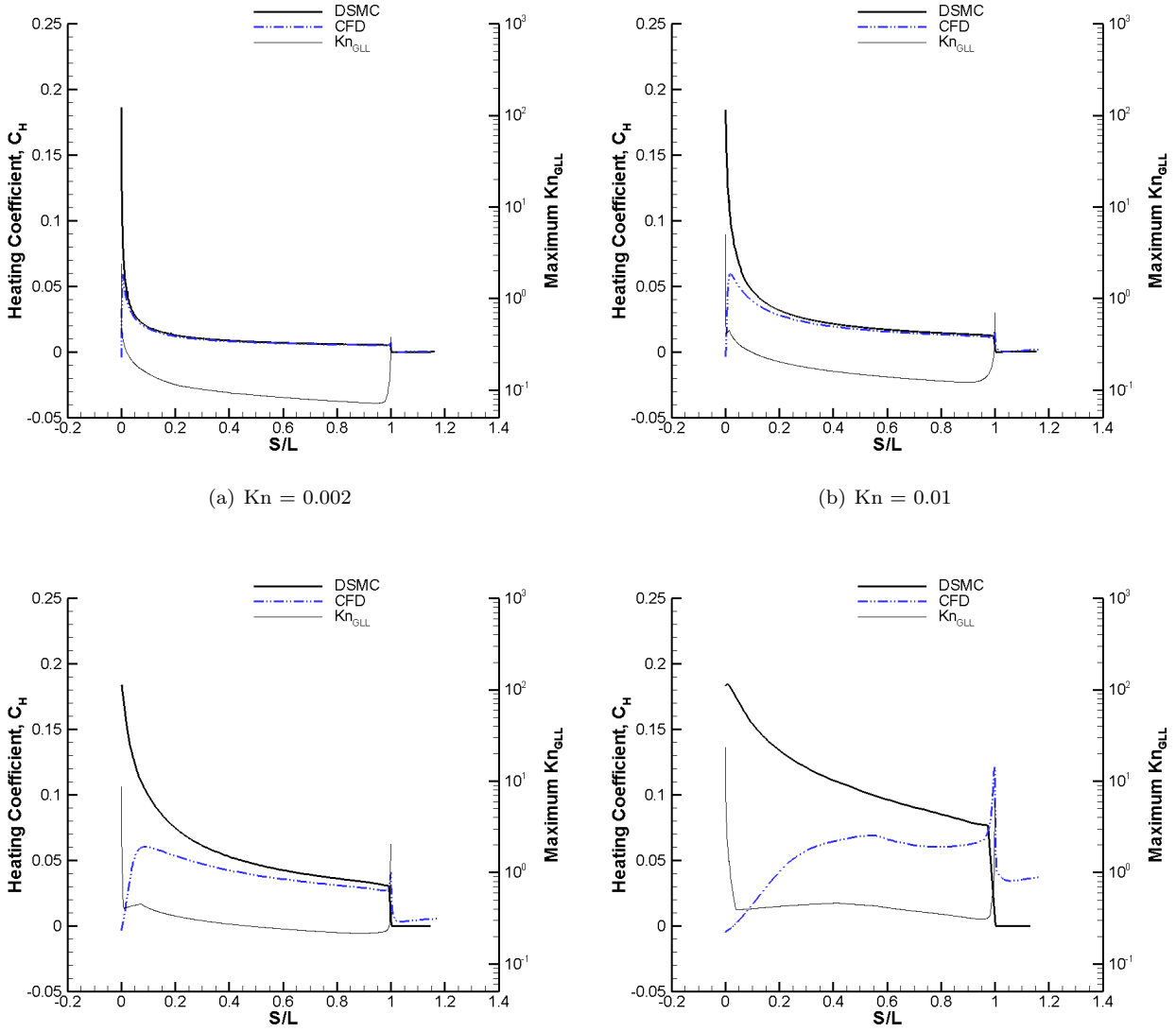

(a) Kn = 0.002

(b) Kn = 0.01

(c) Kn = 0.05

(d) Kn = 0.25

Figure 9. Surface heating coefficient for Mach 10 flow of argon about a wedge. The maximum value of $\mathrm{Kn}_{\mathrm{GLL}}$ near the surface plotted on the right axis. The distance along the surface (including the base), S, is normalized by the top surface length, L.

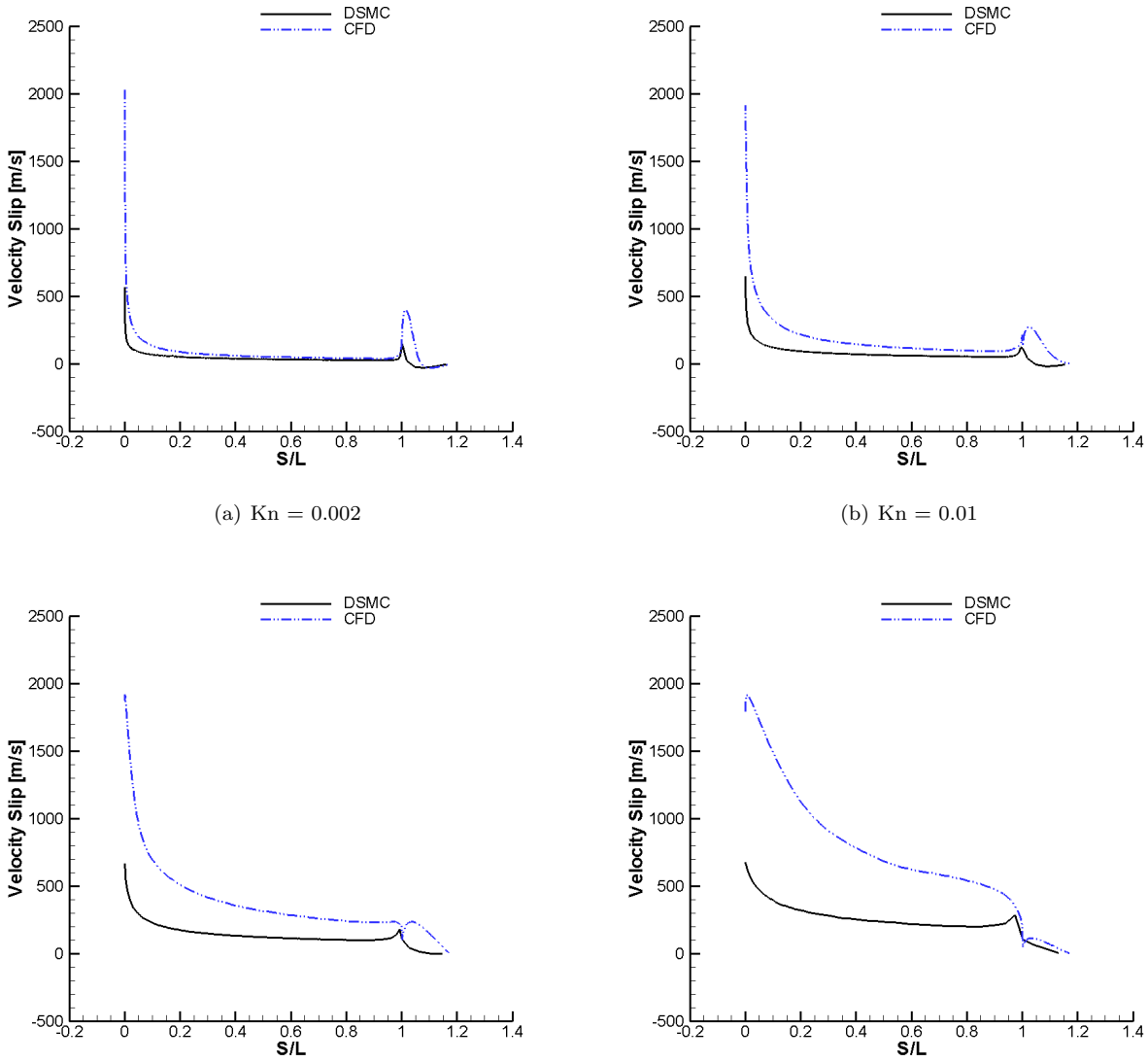

(a) Kn = 0.002

(b) Kn = 0.01

(c) Kn = 0.05

(d) Kn = 0.25

Figure 10. Velocity slip for a Mach 10 flow of argon about a wedge. The distance along the surface (including the base), S, is normalized by the top surface length, L.

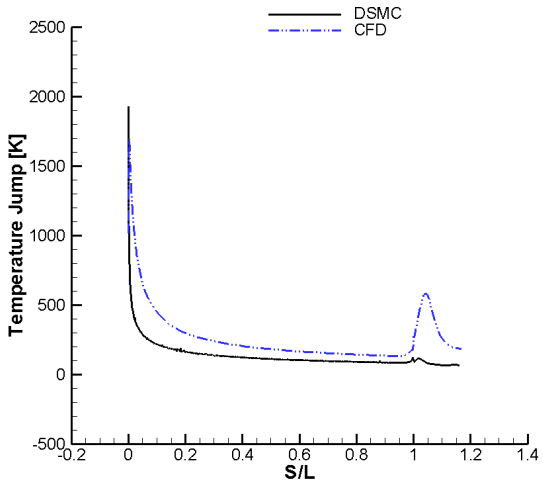

(a) Kn = 0.002

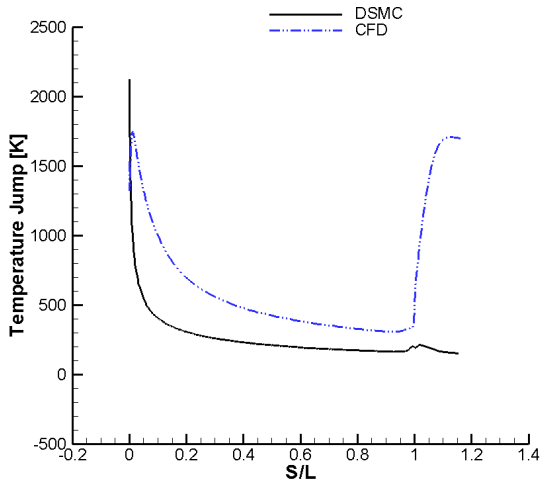

(b) Kn = 0.01

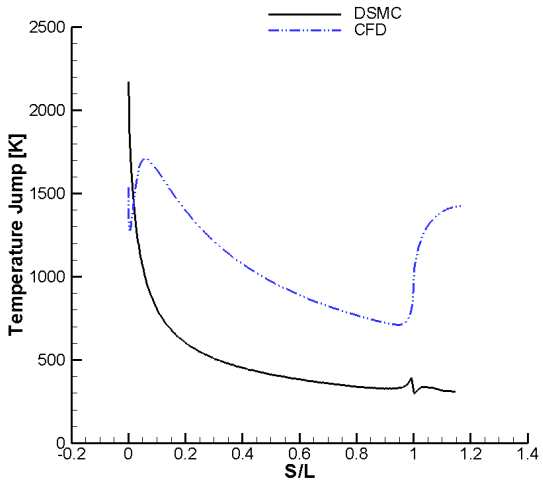

(c) Kn = 0.05

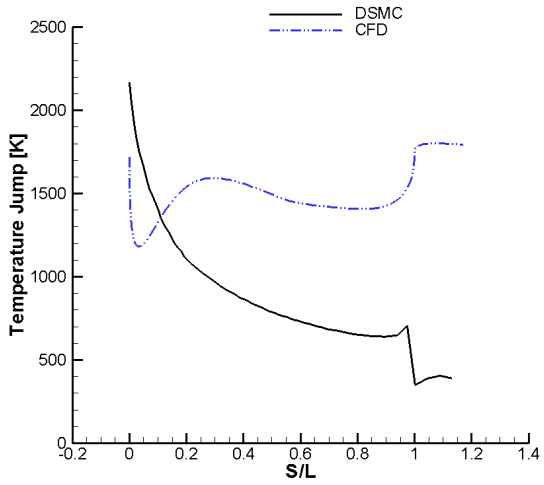

(d) Kn = 0.25

Figure 11. Temperature jump for a Mach 10 flow of argon about a wedge. The distance along the surface (including the base), S, is normalized by the top surface length, L.

IV. Nitrogen

The flow of nitrogen about the wedge is now considered. Table 6 summarizes the total drag predicted by CFD and DSMC. Again, there is reasonable agrement at the lowest Knudsen number, with less than 2% difference for Mach 10, but with a little more than 3% for Mach 25. As the flow becomes more rarefied, the differences increase, although the maximum differences of about 13% and 18% at Kn = 0.25 are lower than that seen with argon.

Table 6. Total drag for flow of nitrogen about a wedge.

Kn_∞	**Mach 10**			**Mach 25**		
	Drag/Length [N/m] (% Difference)					
	DSMC	CFD		DSMC	CFD	
0.002	29.92	30.34	(1.4%)	183.8	189.9	(3.3%)
0.01	10.48	10.86	(3.6%)	67.82	72.34	(6.7%)
0.05	3.946	4.255	(7.8%)	26.10	29.03	(11.2%)
0.25	1.364	1.547	(13.4%)	8.488	10.05	(18.4%)

Figure 12 again illustrates the percentage of total drag due to pressure and friction forces, for both DSMC and CFD. The amount of drag due to friction again ranges from around 50% for Mach 10, Kn = 0.002, to about 90% for Mach 25, Kn = 0.25. A slightly larger percentage of the drag is due to friction at the higher velocity, as was seen with argon, and the contribution of friction forces to the total drag also increases with increasing Knudsen number. It is also shown in Figure 13, that the difference in predicted total drag between CFD and DSMC is due mostly to the differences predicted in the friction forces. Note, however, that the differences due to pressure drag are much lower than was the case with argon; for instance, the argon case for Mach 25, Kn = 0.25 case had a difference of over 5% in the pressure drag prediction (see Figure 2), while the currently considered cases show a maximum of only about 2% for the same Mach and Knudsen numbers. The pressure drag differences for the Mach 10 nitrogen cases are insignificant.

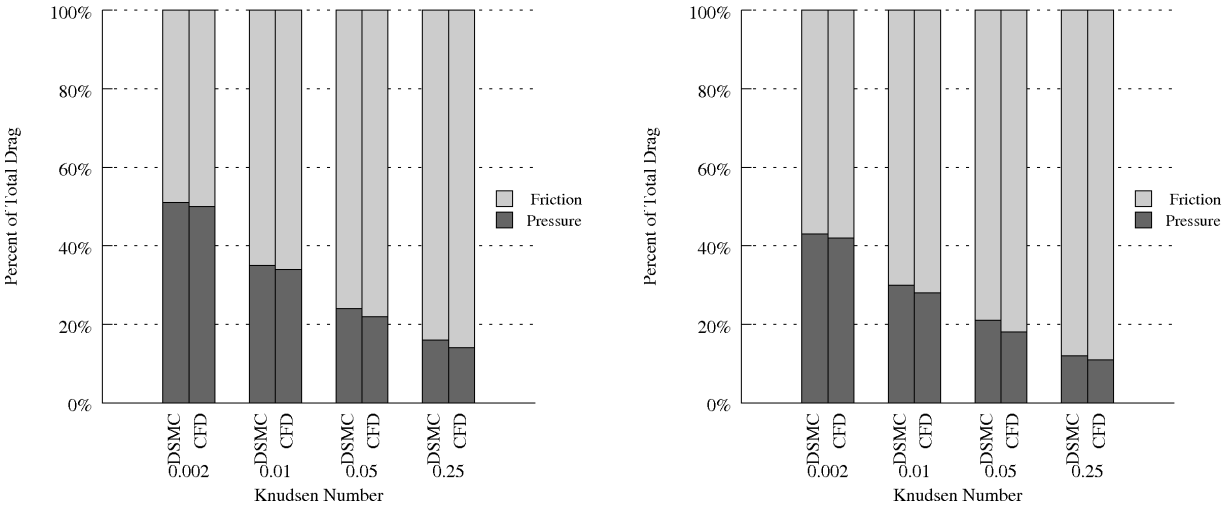

(a) Mach 10 (b) Mach 25

Figure 12. Percentage of total drag due to pressure and friction for flow of nitrogen about a wedge. In contrast to the cylinder cases, here friction forces account for most of the drag.

Peak heating rates for the nitrogen cases are summarized in Table 7, and illustrated graphically in Figure 14. Similar to the argon cases, the error in peak heating is about 70% for most cases, and decreases to about 40% and 25% for Mach 10 and Mach 25, respectively. Again, though, the decrease in peak heating

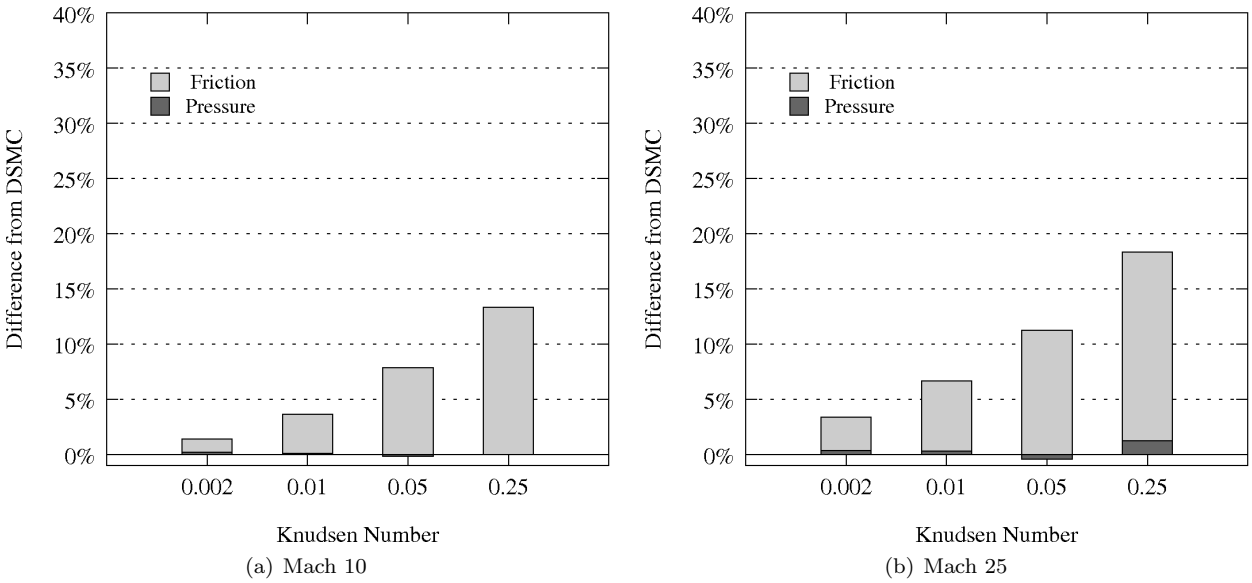

(a) Mach 10 (b) Mach 25

Figure 13. Total drag difference from DSMC predicted by CFD for flow of nitrogen about a wedge.

differences is due to CFD's prediction of peak heating occurring at the wedge shoulder rather than at the leading edge—the actual error at the leading edge is nearly 100%.

Table 7. Peak heat transfer rate for flow of nitrogen about a wedge. The large differences between CFD and DSMC are due to the failure of CFD to predict the high temperatures at the leading edge.

Kn_∞	**Mach 10**			**Mach 25**		
	Peak Heating $[kW/m^2]$ (% Difference)					
	DSMC	CFD		DSMC	CFD	
0.002	209.7	56.76	(-72.9%)	3333.	869.5	(-73.9%)
0.01	41.84	11.46	(-72.6%)	663.1	172.9	(-73.9%)
0.05	8.329	2.308	(-72.3%)	132.8	36.62	(-72.4%)
0.25	1.694	1.032	(-100%)	27.31	20.89	(-100%)

A. Continuum Breakdown

Again, the breakdown parameter is calculated using both the CFD and the DSMC solutions according to Equation 1. Continuum breakdown is expected near the leading edge and in the wake, as was the case for the flow of argon, with the degree of nonequilibrium increasing with increasing Knudsen number.

The locations and values of the breakdown parameter are very similar to what was seen for argon. A large degree of nonequilibrium is predicted near the leading edge and the wedge shoulder, and as the flow becomes more rarefied, the regions where the continuum breakdown parameter exceeds the critical value of 0.05 grow until nearly all of the computational domain is expected to require DSMC for accurate modeling.

B. Flow Field Properties

The translational/rotational temperature fields predicted by both CFD and DSMC for Mach 25 can be seen in Figure 15. Although DSMC simulates complete thermal nonequilibrium, including separate translational and rotational temperatures, here these temperatures are averaged together (weighted by the degrees-of-freedom)

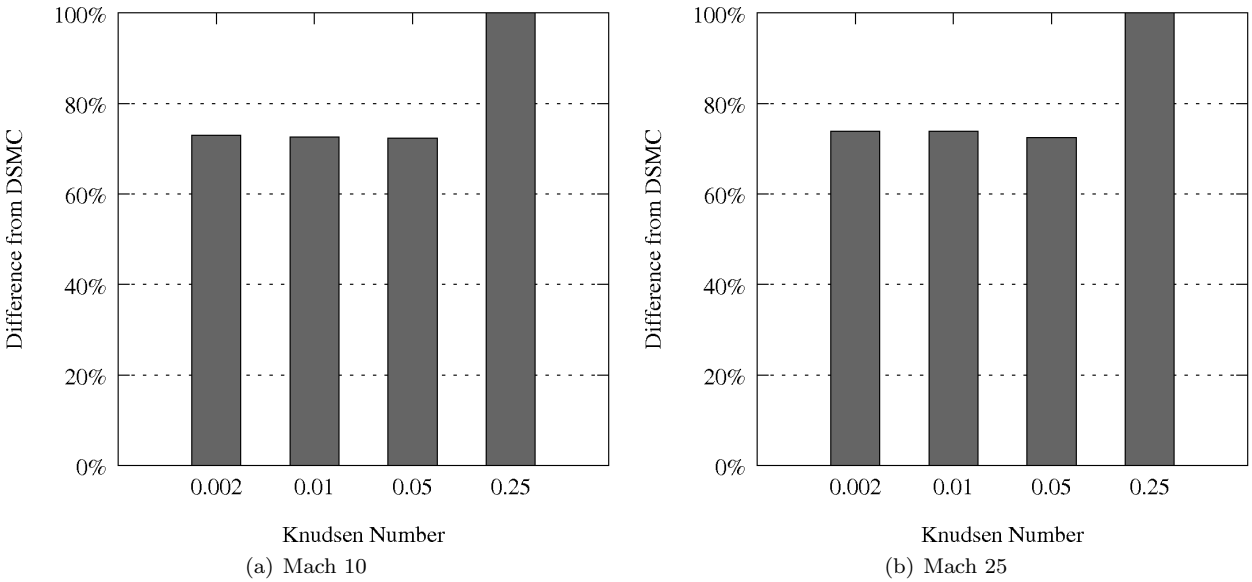

(a) Mach 10 (b) Mach 25

Figure 14. Peak heat transfer rate difference from DSMC predicted by CFD for flow of nitrogen about a wedge. The large differences in peak heating are due to the failure of CFD to predict the high temperatures at the leading edge.

to better compare to the single translational/rotational temperature modeled in the CFD simulations. The area of most concern is near the leading edge where DSMC predicts a higher temperature than does CFD. Although the peak temperatures in the nitrogen flows are lower than those in the argon flows (around 1,700-1,900 K for Mach 10 and 9,000-10,000 K for Mach 25), CFD again underpredicts the temperature by about 40-50%. Similarly to argon, DSMC always predicts the peak temperature to be at the leading edge, while CFD predicts a higher temperature in the wake for these most rarefied cases.

Due to the additional internal energy modes present in a diatomic gas such as nitrogen, a vibrational temperature is also modeled for the wedge. The vibrational temperature fields for Mach 25 are shown in Figure 17. For Mach 10, the maximum vibrational temperature is near the wall temperature of 500 K, again indicating (along with the relatively low translational/rotational temperatures of approximately 2,000 K) that the vibrational modes are only activated due to the wall boundary conditions.

The Mach 25 cases do exhibit some vibrational excitation due to elevated temperatures; the peak vibrational temperature is about 1,800 K for the Mach 25, Kn = 0.002 case. Here it is also seen that DSMC predicts a higher level of vibrational activation than does CFD. This is most likely due to the method used to adjust the DSMC vibrational collision probability to match the theoretical vibrational collision probability.[12] The DSMC vibrational collision probability is multiplied by a correction factor based on the maximum translational temperature seen in the flow field. Here, the maximum translational temperatures are approximately 10,000 K, and a correction factor of 1.43 is used. However, the maximum vibrational temperatures are not near the leading edge of the wedge, but further back along the surface where the translational/rotational temperatures are much lower, around 4,000-5,000 K. The DSMC vibrational collision probability for temperatures in that range are higher than the theoretical model; thus the correction factor should be smaller than unity (around 0.79), rather than larger. Nevertheless, vibrational temperature differences do not seem to affect the surface properties significantly.

C. Surface Properties

The surface property distributions (pressure, shear stress and heat flux) for the nitrogen cases are very similar to those for argon. The overall CFD pressure distribution agrees qualitatively with DSMC for all but the Kn = 0.25 case, but the peak pressure at the leading edge is overpredicted by CFD. The distributions also start to differ in the wake for Kn = 0.05 and Kn = 0.25, with CFD predicting a large spike in the pressure at $S/L = 1$ as the flow begins to expand into the wake. In all cases, CFD tends to overpredict the pressure and there is some effect of the pressure on the overall overprediction of total drag by CFD, although this

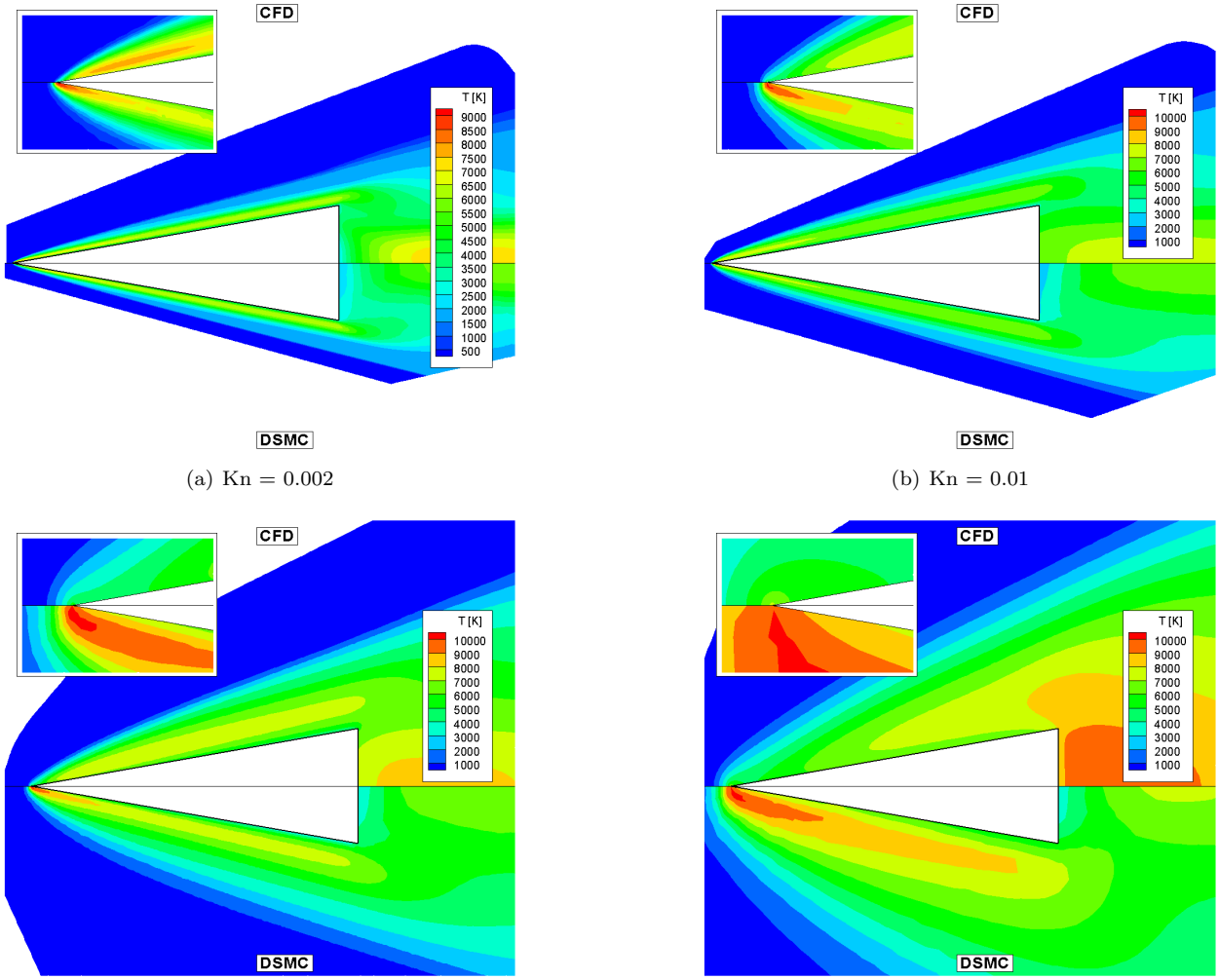

(a) Kn = 0.002

(b) Kn = 0.01

(c) Kn = 0.05

(d) Kn = 0.25

Figure 15. Translational/rotational temperature field for a Mach 25 flow of nitrogen about a wedge. DSMC predicts a much higher temperature than CFD near the leading edge (inset). Note that CFD predicts a higher temperature in the wake than near the leading edge for Kn = 0.25, while DSMC predicts a maximum temperature at the leading edge.

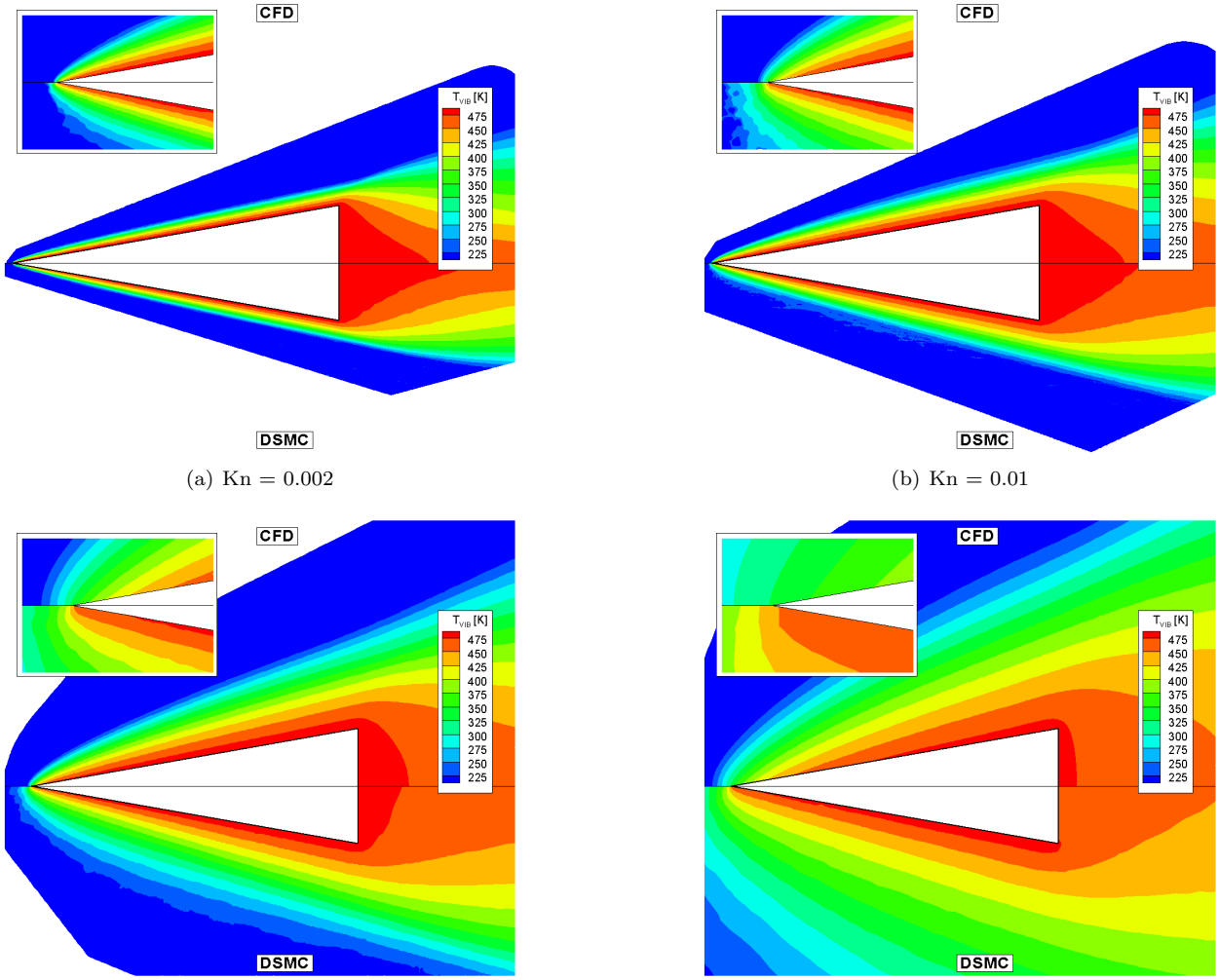

(a) Kn = 0.002

(b) Kn = 0.01

(c) Kn = 0.05

(d) Kn = 0.25

Figure 16. Vibrational temperature field for a Mach 10 flow of nitrogen about a wedge. Note that the vibrational activation is due to the wall vibrational temperature of 500 K.

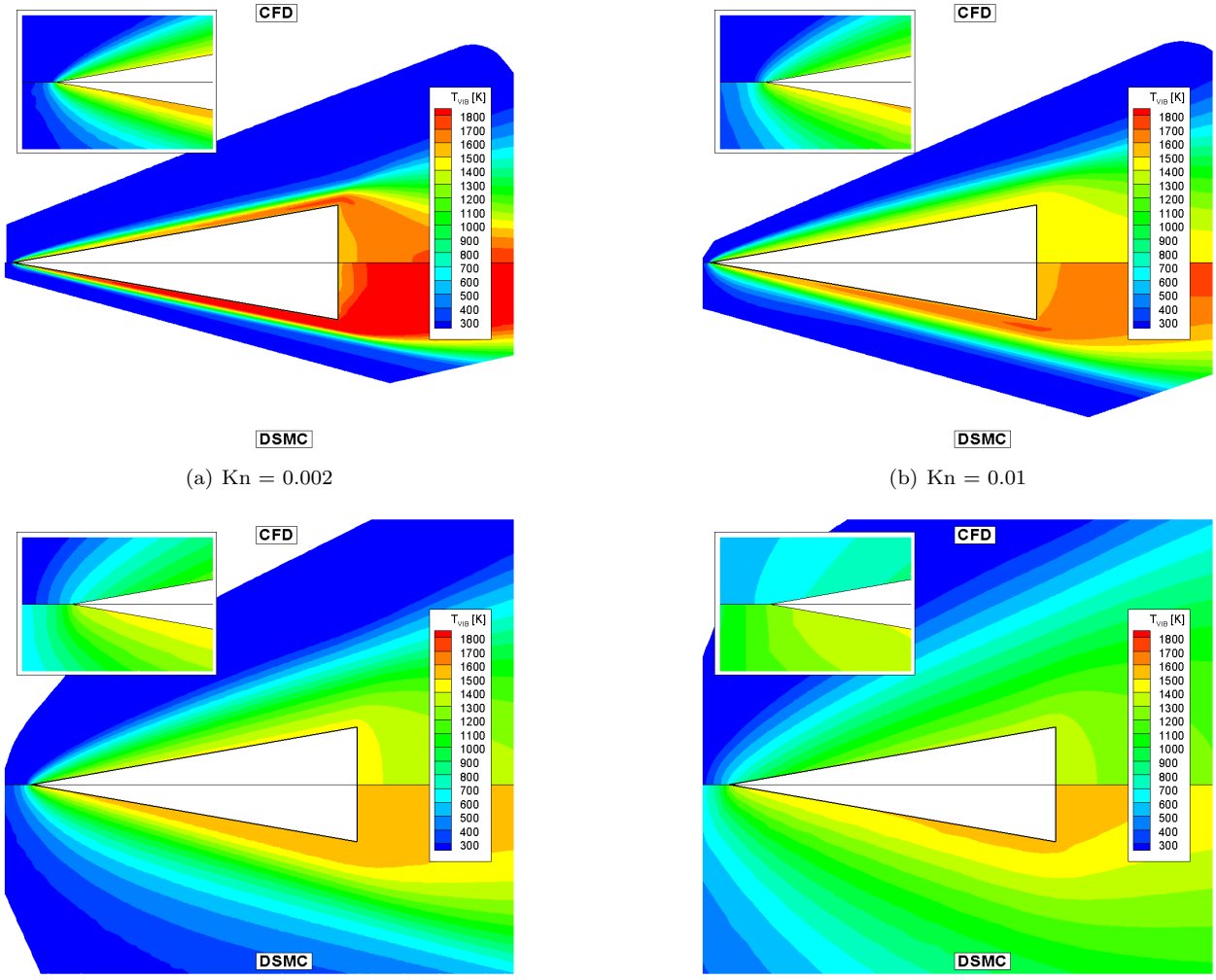

(a) Kn = 0.002

(b) Kn = 0.01

(c) Kn = 0.05

(d) Kn = 0.25

Figure 17. Vibrational temperature field for a Mach 25 flow of nitrogen about a wedge. Note that the wall vibrational temperature is 1500 K.

effect is not as great as that of shear stress, as was shown in Figure 13.

The shear stress profiles for the nitrogen simulations are also very similar to those for the argon simulations. The CFD results show a large spike at the leading edge that does not significantly affect the total drag. Other than this peak at the leading edge, there are fewer differences in the shear stress than there were for the pressure. However, the total drag is affected most by the friction forces. Again, this is explained by noting the much larger effect that shear stress has on the total drag as seen in Figure 2.

Plots for the accumulated total drag along the wedge surface (not shown) due to both friction and pressure forces for the nitrogen cases also demonstrate that the differences in friction drag for Kn = 0.002 and Kn = 0.01 occur along the first 20% of the wedge surface. For Kn = 0.05, the area where the difference accumulates most is in the first 40-50% of the wedge surface; and for Kn = 0.25, the differences accumulate mostly between 20% and 80% of the wedge length. The same trends are noted with nitrogen as they were with argon:

- The large value of skin friction coefficient at the leading edge does not significantly affect the total drag.
- The contribution of friction forces to the total drag increases as the density decreases.
- There is no contribution to total drag due to friction forces in the wake.
- Pressure forces on the base of the wedge (in the wake) decrease the total drag.
- There is little disagreement in the predictions of total drag due to pressure forces for most cases.

Additionally, the good agreement between drag due to pressure, as Figure 13 shows, is not due to perfect agreement between the pressure distributions along the entire surface (as discussed above). Instead, the accumulated drag due to pressure does show some differences along the surface, but the final total values happen to agree.

The heat transfer rate distributions (not shown)are also similar to those for argon, although a larger heat flux coefficient is predicted for nitrogen. The peak DSMC heating coefficients remain near 0.22, and the peak CFD heating coefficients remain well under 0.1. Thus, the difference in heating rate is also around 70% for most of the cases. For Kn = 0.25, CFD predicts a peak heating rate at the shoulder, with no heating predicted at the leading edge. Thus, the actual error in heating rate prediction is much greater than the 40% and 25% cited in Table 7.

D. Slip Quantities

The velocity slip along the wedge surface is very similar to those obtained with argon and are not shown here. CFD predicts a peak velocity slip between 2,000-2,500 m/s for Mach 10 and between 5000-6,000 m/s for Mach 25 near the leading edge, while DSMC predicts a maximum velocity slip of about 750 m/s for Mach 10 and about 1,500 m/s for Mach 25. For Kn = 0.002, Kn = 0.01 and even Kn = 0.05 to some extent, CFD qualitatively agrees fairly well with DSMC. However, for Kn = 0.25 this agreement worsens considerably. Once again, the locations where the disagreement is most apparent, at and near the leading edge, are also the locations where the shear stress distributions differ the most. Thus, there is a good correlation between velocity slip disagreement and shear stress disagreement.

The translational/rotational temperature jump profiles for nitrogen flows, shown in Figure 18 for Mach 25, are qualitatively similar to the temperature jump profiles obtained for argon, with the additional distinction of the rotational-translational nonequilibrium in the DSMC data. The translational and rotational temperature jump profiles from DSMC are shown separately (as colored lines) as well as their DOF-weighted average value (as a black line). Although the peak translational temperature jump values predicted by DSMC are nearly 2,000 K for Mach 10 and nearly 10,000 K for Mach 25, which are near those predicted for argon, there is significant thermal nonequilibrium and the rotational temperature jump is much lower than the translational temperature jump; at the leading edge, the rotational temperature jump is negative. For Kn = 0.05 and Kn = 0.25, the translational and rotational temperatures along the surface never do fully equilibrate, although they are closer to equilibrium at the base of the wedge. Nevertheless, CFD agrees moderately well with the averaged translational/rotational temperature jump predicted by DSMC for the lower Knudsen number flows for Mach 10; there is more disagreement for Mach 25.

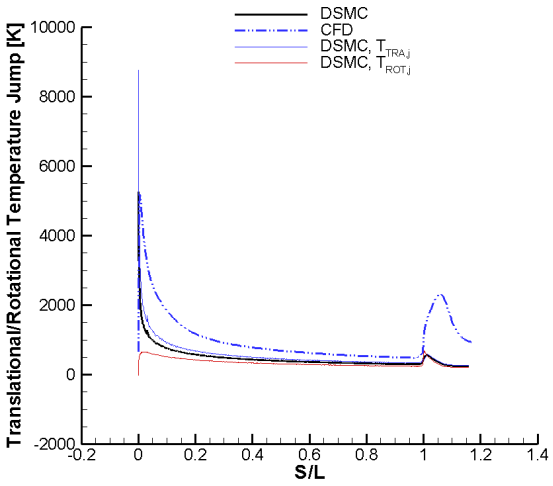

(a) Kn = 0.002

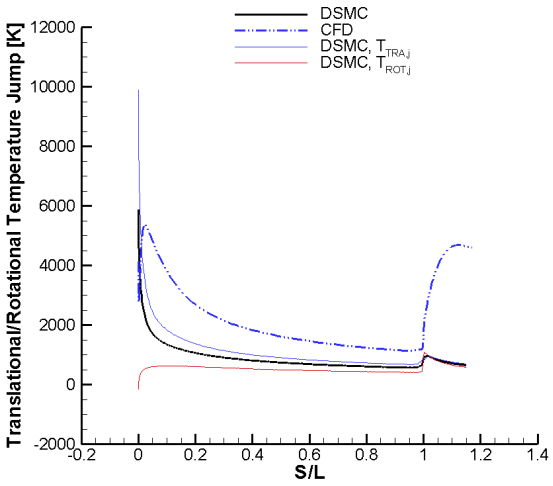

(b) Kn = 0.01

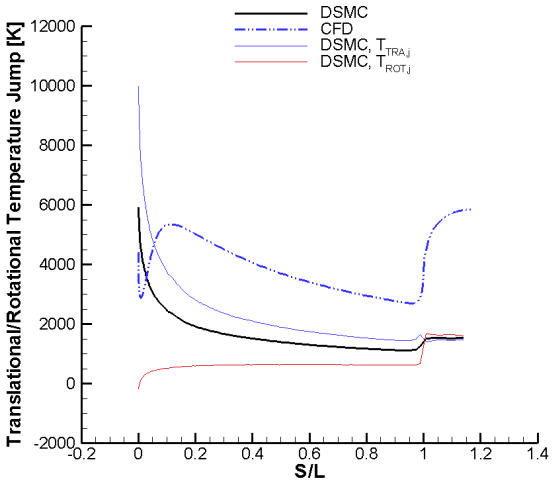

(c) Kn = 0.05

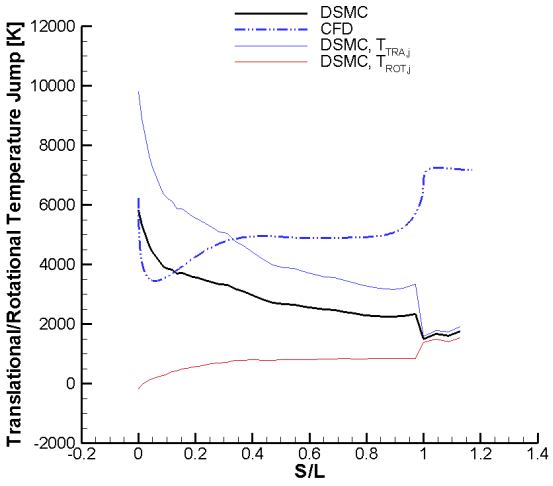

(d) Kn = 0.25

Figure 18. Translational/rotational temperature jump for a Mach 25 flow of nitrogen about a wedge. The separate translational and rotational temperature jumps from DSMC are plotted along with the average temperature jump from CFD and DSMC. The distance along the surface (including the base), S, is normalized by the top surface length, L.

The vibrational temperature jump profiles for Mach 25 are in Figure 19. For Mach 10, there is very little vibrational excitation and the vibrational temperature jump predicted by both methods is near zero, except at the leading edge where CFD overpredicts the amount of vibrational temperature slip. The Kn = 0.25 case is an exception, where DSMC predicts a small, negative, temperature jump value. For Mach 25, the situation is very similar to that for Mach 10, with the exception that the differences between CFD and DSMC are more pronounced for Kn = 0.01 and Kn = 0.05.

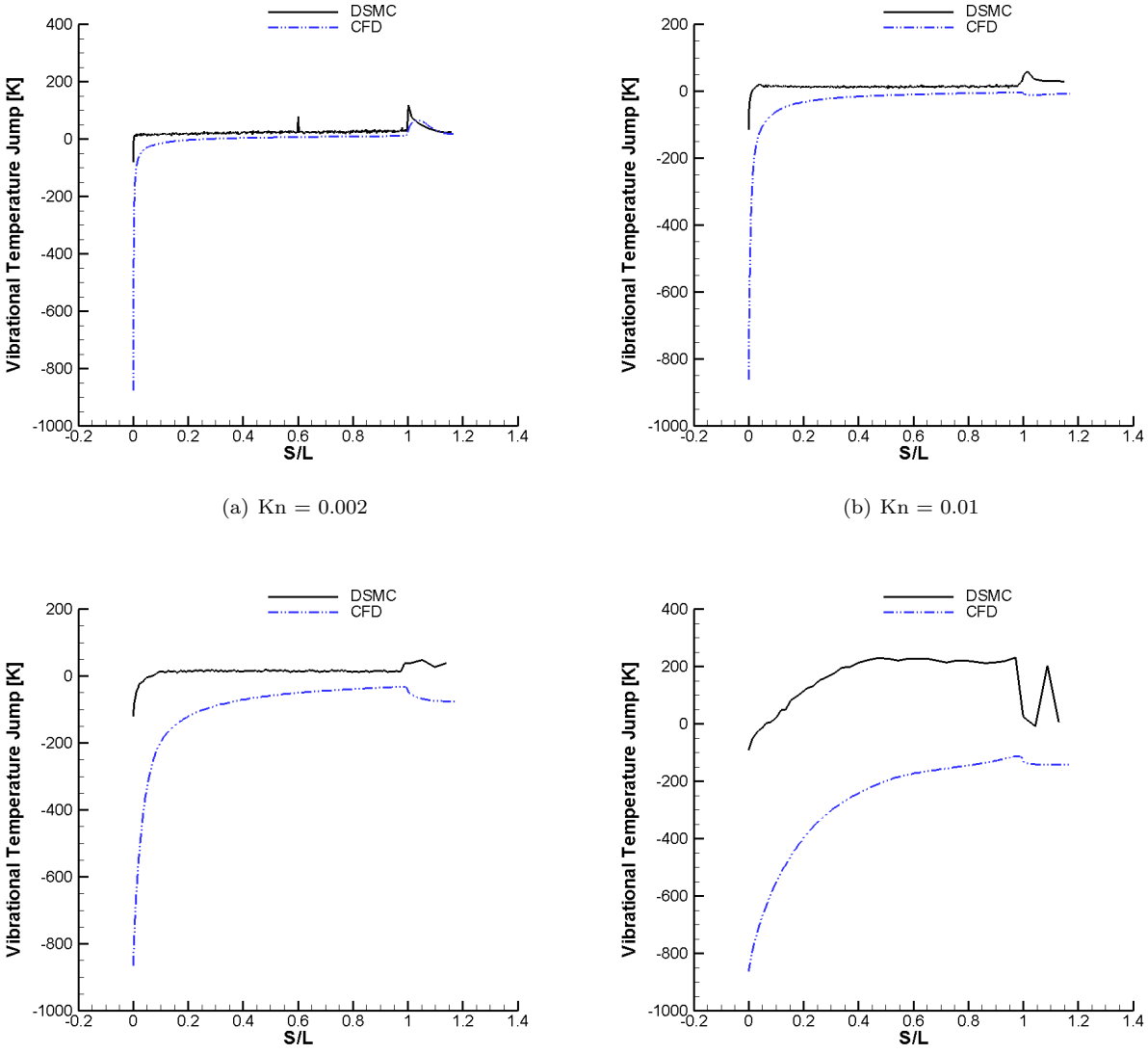

(a) Kn = 0.002

(b) Kn = 0.01

(c) Kn = 0.05

(d) Kn = 0.25

Figure 19. Vibrational temperature jump for a Mach 25 flow of nitrogen about a wedge. The distance along the surface (including the base), S, is normalized by the top surface length, L.

V. Summary

The sharp-leading edge geometry of the wedge leads to additional flow phenomena not seen with the cylinder, which in turn affect the surface property predictions.

The differences in total drag predicted by CFD and DSMC are greater than they were with the cylinder geometry, due to the larger effect of the friction forces on the drag. Additionally, there are greater differences

in the pressure profiles along the wedge surface, but the effect on total drag is relatively small (due to the small angle of the surface with the flow).

The amount of nonequilibrium near the leading-edge significantly affects the prediction of temperature gradients, and thus there are significant differences in the heat transfer rate predictions–CFD fails to adequately predict the large heat fluxes near the leading edge of an infinitely-sharp wedge.

As with the blunt body cases previously studied, there are no significant differences between the nitrogen and argon flows, despite the additional presence of thermal nonequilibrium for the diatomic gas.

VI. Acknowledgments

This work was sponsored in part by the Space Vehicle Technology Institute, under NASA grant NCC3-989 with joint sponsorship from the U.S. Department of Defense and the U.S. Air Force Office of Scientific Research through grant FA9550-05-1-0115.

References

[1]Bird, G. A. Breakdown of translational and rotational equilibrium in gaseous expansions. *AIAA Journal 8*, 11 (1970), 1998–2003.

[2]Bird, G. A. *Gas Dynamics and the Direct Simulation of Gas Flows*. Oxford University Press, Oxford, 1994.

[3]Blottner, F. G., Johnson, M., and Ellis, M. Chemically reacting viscous flow program for multi-component gas mixtures. Tech. Rep. SC-RR-70-754, Sandia Laboratories, Albuquerque, New Mexico, 1971.

[4]Boyd, I. D. Analysis of rotational nonequilibrium in standing shock waves of nitrogen. *AIAA Journal 28*, 11 (Nov. 1990), 1997–1999.

[5]Boyd, I. D., Chen, G., and Candler, G. V. Predicting failure of the continuum fluid equations in transitional hypersonic flows. *Physics of Fluids 7*, 1 (Jan. 1995), 210–219.

[6]Camberos, J. A., Schrock, C. R., McMullan, R. J., and Branam, R. D. Development of continuum onset criteria with direct simulation Monte-Carlo using Boltzmann's H-Theorem: Review and vision. In *Proceedings of the 9th AIAA/ASME Joint Thermophysics and Heat Transfer Conference* (San Francisco, California, June 2006).

[7]Dietrich, S., and Boyd, I. D. Scalar and parallel optimized implementation of the direct simulation Monte Carlo method. *Journal of Computational Physics 126*, 2 (1996), 328–342.

[8]Garcia, A. L., Bell, J. B., Crutchfield, W. Y., and Alder, B. J. Adaptive mesh and algorithm refinement using direct simulation Monte Carlo. *Journal of Computational Physics 154* (1999), 134.

[9]Gökçen, T., and MacCormack, R. W. Nonequilibrium effects for hypersonic transitional flows using continuum approach. AIAA Paper 1989–0461.

[10]Koura, K., and Matsumoto, H. Variable soft sphere molecular model for air species. *Physics of Fluids A 4*, 5 (May 1992), 1083–1085.

[11]Lofthouse, A. J., Boyd, I. D., and Wright, M. J. Effects of continuum breakdown on hypersonic aerothermodynamics. *Physics of Fluids 19*, 2 (2007), 027105.

[12]Lofthouse, A. J., Scalabrin, L. C., and Boyd, I. D. Hypersonic aerothermodynamics analysis across nonequilibrium regimes using continuum and particle methods. AIAA Paper 2007–3903.

[13]Lofthouse, A. J., Scalabrin, L. C., and Boyd, I. D. Velocity slip and temperature jump in hypersonic aerothermodynamics. *Journal of Thermophysics and Heat Transfer 22*, 1 (2008), 38–49.

[14]Millikan, R. C., and White, D. R. Systematics of vibrational relaxation. *Journal of Chemical Physics 39* (1963), 2309–3213.

[15]Park, C. *Nonequilibrium Hypersonic Aerothermodynamics*. John Wiley & Sons, 1990.

[16]Scalabrin, L. C., and Boyd, I. D. Development of an unstructured Navier-Stokes solver for hypersonic nonequilibrium aerothermodynamics. AIAA Paper 2005–5203.

[17]Scalabrin, L. C., and Boyd, I. D. Numerical simulation of weakly ionized hypersonic flow for reentry configurations. AIAA Paper 2006–3773.

[18]Schwartzentruber, T. E., Scalabrin, L. C., and Boyd, I. D. Hybrid particle-continuum simulations of nonequilibrium hypersonic blunt body flow fields. AIAA Paper 2006–3602.

[19]Tiwari, S. Coupling of the Boltzmann and Euler equations with automatic domain decomposition. *Journal of Computational Physics 144* (Aug. 1998), 710–726.

[20]Vijayakumar, P., Sun, Q., and Boyd, I. D. Vibrational-translational energy exchange for the direct simulation Monte Carlo method. *Physics of Fluids 11*, 8 (Aug. 1999), 2117–2126.

[21]Vincenti, W. G., and C. H. Kruger, J. *Introduction to Physical Gas Dynamics*. Krieger Publishing Company, 1965.

[22]Wang, W.-L. *A Hybrid Particle/Continuum Approach for Nonequilibrium Hypersonic Flows*. PhD thesis, The University of Michigan, 2004.

[23]Wilke, C. R. A viscosity equation for gas mixtures. *Journal of Chemical Physics 18*, 4 (Apr. 1950), 517–519.